

Search for Bottomonium States in Exclusive Radiative $\Upsilon(2S)$ Decays

S. Sandilya,⁵⁴ K. Trabelsi,¹² G. B. Mohanty,⁵⁴ I. Adachi,¹² H. Aihara,⁵⁹ D. M. Asner,⁴⁵ T. Aushev,²⁰ T. Aziz,⁵⁴ A. M. Bakich,⁶⁸ A. Bala,⁴⁶ V. Bhardwaj,³⁷ B. Bhuyan,¹⁵ A. Bondar,³ G. Bonvicini,⁶⁵ A. Bozek,⁴⁰ M. Bračko,^{30,21} T. E. Browder,¹¹ P. Chen,³⁹ B. G. Cheon,¹⁰ K. Chilikin,²⁰ R. Chistov,²⁰ K. Cho,²⁴ V. Chobanova,³¹ S.-K. Choi,⁹ Y. Choi,⁵² D. Cinabro,⁶⁵ J. Dalseno,^{31,55} J. Dingfelder,² Z. Doležal,⁴ A. Drutskoy,^{20,33} D. Dutta,¹⁵ S. Eidelman,³ H. Farhat,⁶⁵ J. E. Fast,⁴⁵ M. Feindt,²³ T. Ferber,⁶ A. Frey,⁸ V. Gaur,⁵⁴ N. Gabyshev,³ S. Ganguly,⁶⁵ R. Gillard,⁶⁵ Y. M. Goh,¹⁰ B. Golob,^{28,21} J. Haba,¹² T. Hara,¹² K. Hayasaka,³⁶ H. Hayashii,³⁷ Y. Hoshi,⁵⁷ W.-S. Hou,³⁹ Y. B. Hsiung,³⁹ H. J. Hyun,²⁶ T. Iijima,^{36,35} A. Ishikawa,⁵⁸ R. Itoh,¹² Y. Iwasaki,¹² T. Julius,³² D. H. Kah,²⁶ J. H. Kang,⁶⁷ E. Kato,⁵⁸ H. Kawai,⁵ T. Kawasaki,⁴² C. Kiesling,³¹ D. Y. Kim,⁵¹ H. O. Kim,²⁶ J. B. Kim,²⁵ J. H. Kim,²⁴ Y. J. Kim,²⁴ J. Klucar,²¹ B. R. Ko,²⁵ P. Kodyš,⁴ S. Korpar,^{30,21} P. Križan,^{28,21} P. Krokovny,³ T. Kumita,⁶¹ A. Kuzmin,³ Y.-J. Kwon,⁶⁷ J. S. Lange,⁷ S.-H. Lee,²⁵ J. Li,⁵⁰ Y. Li,⁶⁴ J. Libby,¹⁶ Z. Q. Liu,¹⁷ D. Liventsev,¹² P. Lukin,³ J. MacNaughton,¹² D. Matvienko,³ K. Miyabayashi,³⁷ H. Miyata,⁴² R. Mizuk,^{20,33} A. Moll,^{31,55} N. Muramatsu,⁴⁸ R. Mussa,¹⁹ Y. Nagasaka,¹³ M. Nakao,¹² M. Nayak,¹⁶ C. Ng,⁵⁹ N. K. Nisar,⁵⁴ S. Nishida,¹² O. Nitoh,⁶² S. Ogawa,⁵⁶ S. Okuno,²² C. Oswald,² G. Pakhlova,²⁰ C. W. Park,⁵² H. Park,²⁶ H. K. Park,²⁶ T. K. Pedlar,²⁹ R. Pestotnik,²¹ M. Petrič,²¹ L. E. Piilonen,⁶⁴ M. Ritter,³¹ M. Röhrken,²³ A. Rostomyan,⁶ S. Ryu,⁵⁰ H. Sahoo,¹¹ T. Saito,⁵⁸ K. Sakai,¹² Y. Sakai,¹² L. Santelj,²¹ T. Sanuki,⁵⁸ Y. Sato,⁵⁸ V. Savinov,⁴⁷ O. Schneider,²⁷ G. Schnell,^{1,14} D. Semmler,⁷ K. Senyo,⁶⁶ M. E. Sevier,³² M. Shapkin,¹⁸ C. P. Shen,³⁵ T.-A. Shibata,⁶⁰ J.-G. Shiu,³⁹ B. Shwartz,³ A. Sibidanov,⁶⁸ F. Simon,^{31,55} Y.-S. Sohn,⁶⁷ A. Sokolov,¹⁸ E. Solovieva,²⁰ S. Stanič,⁴³ M. Starič,²¹ M. Steder,⁶ T. Sumiyoshi,⁶¹ U. Tamponi,^{19,63} K. Tanida,⁵⁰ G. Tatishvili,⁴⁵ Y. Teramoto,⁴⁴ T. Tsuboyama,¹² M. Uchida,⁶⁰ S. Uehara,¹² T. Uglov,^{20,34} Y. Unno,¹⁰ S. Uno,¹² P. Urquijo,² S. E. Vahsen,¹¹ C. Van Hulse,¹ P. Vanhoefer,³¹ G. Varner,¹¹ V. Vorobyev,³ M. N. Wagner,⁷ C. H. Wang,³⁸ M.-Z. Wang,³⁹ P. Wang,¹⁷ X. L. Wang,⁶⁴ M. Watanabe,⁴² Y. Watanabe,²² J. Wiechczynski,⁴⁰ K. M. Williams,⁶⁴ E. Won,²⁵ B. D. Yabsley,⁶⁸ J. Yamaoka,¹¹ Y. Yamashita,⁴¹ S. Yashchenko,⁶ C. Z. Yuan,¹⁷ Y. Yusa,⁴² C. C. Zhang,¹⁷ Z. P. Zhang,⁴⁹ V. Zhilich,³ and A. Zupanc²³

(The Belle Collaboration)

¹University of the Basque Country UPV/EHU, 48080 Bilbao

²University of Bonn, 53115 Bonn

³Budker Institute of Nuclear Physics SB RAS and Novosibirsk State University, Novosibirsk 630090

⁴Faculty of Mathematics and Physics, Charles University, 121 16 Prague

⁵Chiba University, Chiba 263-8522

⁶Deutsches Elektronen-Synchrotron, 22607 Hamburg

⁷Justus-Liebig-Universität Gießen, 35392 Gießen

⁸II. Physikalisches Institut, Georg-August-Universität Göttingen, 37073 Göttingen

⁹Gyeongsang National University, Chinju 660-701

¹⁰Hanyang University, Seoul 133-791

¹¹University of Hawaii, Honolulu, Hawaii 96822

¹²High Energy Accelerator Research Organization (KEK), Tsukuba 305-0801

¹³Hiroshima Institute of Technology, Hiroshima 731-5193

¹⁴Ikerbasque, 48011 Bilbao

¹⁵Indian Institute of Technology Guwahati, Assam 781039

¹⁶Indian Institute of Technology Madras, Chennai 600036

¹⁷Institute of High Energy Physics, Chinese Academy of Sciences, Beijing 100049

¹⁸Institute for High Energy Physics, Protvino 142281

¹⁹INFN - Sezione di Torino, 10125 Torino

²⁰Institute for Theoretical and Experimental Physics, Moscow 117218

²¹J. Stefan Institute, 1000 Ljubljana

²²Kanagawa University, Yokohama 221-8686

²³Institut für Experimentelle Kernphysik, Karlsruher Institut für Technologie, 76131 Karlsruhe

²⁴Korea Institute of Science and Technology Information, Daejeon 305-806

²⁵Korea University, Seoul 136-713

²⁶Kyungpook National University, Daegu 702-701

²⁷École Polytechnique Fédérale de Lausanne (EPFL), Lausanne 1015

²⁸Faculty of Mathematics and Physics, University of Ljubljana, 1000 Ljubljana

²⁹Luther College, Decorah, Iowa 52101

³⁰University of Maribor, 2000 Maribor

³¹Max-Planck-Institut für Physik, 80805 München

- ³²*School of Physics, University of Melbourne, Victoria 3010*
³³*Moscow Physical Engineering Institute, Moscow 115409*
³⁴*Moscow Institute of Physics and Technology, Moscow Region 141700*
³⁵*Graduate School of Science, Nagoya University, Nagoya 464-8602*
³⁶*Kobayashi-Maskawa Institute, Nagoya University, Nagoya 464-8602*
³⁷*Nara Women's University, Nara 630-8506*
³⁸*National United University, Miao Li 36003*
³⁹*Department of Physics, National Taiwan University, Taipei 10617*
⁴⁰*H. Niewodniczanski Institute of Nuclear Physics, Krakow 31-342*
⁴¹*Nippon Dental University, Niigata 951-8580*
⁴²*Niigata University, Niigata 950-2181*
⁴³*University of Nova Gorica, 5000 Nova Gorica*
⁴⁴*Osaka City University, Osaka 558-8585*
⁴⁵*Pacific Northwest National Laboratory, Richland, Washington 99352*
⁴⁶*Panjab University, Chandigarh 160014*
⁴⁷*University of Pittsburgh, Pittsburgh, Pennsylvania 15260*
⁴⁸*Research Center for Electron Photon Science, Tohoku University, Sendai 980-8578*
⁴⁹*University of Science and Technology of China, Hefei 230026*
⁵⁰*Seoul National University, Seoul 151-742*
⁵¹*Soongsil University, Seoul 156-743*
⁵²*Sungkyunkwan University, Suwon 440-746*
⁵³*School of Physics, University of Sydney, New South Wales 2006*
⁵⁴*Tata Institute of Fundamental Research, Mumbai 400005*
⁵⁵*Excellence Cluster Universe, Technische Universität München, 85748 Garching*
⁵⁶*Toho University, Funabashi 274-8510*
⁵⁷*Tohoku Gakuin University, Tagajo 985-8537*
⁵⁸*Tohoku University, Sendai 980-8578*
⁵⁹*Department of Physics, University of Tokyo, Tokyo 113-0033*
⁶⁰*Tokyo Institute of Technology, Tokyo 152-8550*
⁶¹*Tokyo Metropolitan University, Tokyo 192-0397*
⁶²*Tokyo University of Agriculture and Technology, Tokyo 184-8588*
⁶³*University of Torino, 10124 Torino*
⁶⁴*CNP, Virginia Polytechnic Institute and State University, Blacksburg, Virginia 24061*
⁶⁵*Wayne State University, Detroit, Michigan 48202*
⁶⁶*Yamagata University, Yamagata 990-8560*
⁶⁷*Yonsei University, Seoul 120-749*
⁶⁸*School of Physics, University of Sydney, NSW 2006*
(Dated: October 9, 2018)

We search for bottomonium states in $\Upsilon(2S) \rightarrow (b\bar{b})\gamma$ decays with an integrated luminosity of 24.7fb^{-1} recorded at the $\Upsilon(2S)$ resonance with the Belle detector at KEK, containing $(157.8 \pm 3.6) \times 10^6$ $\Upsilon(2S)$ events. The $(b\bar{b})$ system is reconstructed in 26 exclusive hadronic final states composed of charged pions, kaons, protons, and K_S^0 mesons. We find no evidence for the state recently observed around 9975 MeV ($X_{b\bar{b}}$) in an analysis based on a data sample of 9.3×10^6 $\Upsilon(2S)$ events collected with the CLEO III detector. We set a 90% confidence level upper limit on the branching fraction $\mathcal{B}[\Upsilon(2S) \rightarrow X_{b\bar{b}}\gamma] \times \sum_i \mathcal{B}[X_{b\bar{b}} \rightarrow h_i] < 4.9 \times 10^{-6}$, summed over the exclusive hadronic final states employed in our analysis. This result is an order of magnitude smaller than the measurement reported with CLEO data. We also set an upper limit for the $\eta_b(1S)$ state of $\mathcal{B}[\Upsilon(2S) \rightarrow \eta_b(1S)\gamma] \times \sum_i \mathcal{B}[\eta_b(1S) \rightarrow h_i] < 3.7 \times 10^{-6}$.

PACS numbers: 14.40.Pq, 13.25.Gv, 12.39.Pn

Bottomonium, a bound system of a bottom (b) quark and its antiquark (\bar{b}), offers a unique laboratory to study strong interactions; since the b quark is heavier than other quarks ($q = u, d, s, c$), the system can be described by nonrelativistic quantum mechanics and effective theories [1]. Spin-singlet states permit the study of spin-spin interactions within the $b\bar{b}$ system.

The ground state of the bottomonium family with zero orbital and spin angular momenta, the $\eta_b(1S)$, was discovered by the BABAR Collaboration in 2008 [2]. Ev-

idence for its radially excited spin-singlet partner, the $\eta_b(2S)$, was reported by the Belle Collaboration [3] using a 133.4fb^{-1} data sample collected near the $\Upsilon(5S)$ resonance. That analysis used the process $e^+e^- \rightarrow \Upsilon(5S) \rightarrow h_b(nP)\pi^+\pi^-$, $h_b \rightarrow \eta_b(mS)\gamma$ for $n(\geq m) = 1, 2$. The $\eta_b(2S)$ mass measured in the $h_b(2P) \rightarrow \eta_b(2S)\gamma$ transition was $[9999.0 \pm 3.5(\text{stat})_{-1.9}^{+2.8}(\text{syst})]\text{MeV}/c^2$, corresponding to a hyperfine mass splitting between $\Upsilon(2S)$ and $\eta_b(2S)$ states, $\Delta M_{\text{HF}}(2S) \equiv M[\Upsilon(2S)] - M[\eta_b(2S)]$, of $[24.3_{-4.5}^{+4.0}]\text{MeV}/c^2$. The BABAR and Belle analyses were

based on an inclusive approach, where the final state of the $\eta_b(nS)$ was not reconstructed.

There is a recent claim [4] of the observation of a bottomonium state $X_{b\bar{b}}$ in the radiative decay $\Upsilon(2S) \rightarrow X_{b\bar{b}}\gamma$ with a data sample of 9.3×10^6 $\Upsilon(2S)$ decays recorded with the CLEO III detector. The analysis, based on the reconstruction of 26 exclusive hadronic final states, reports a mass of $[9974.6 \pm 2.3(\text{stat}) \pm 2.1(\text{syst})] \text{ MeV}/c^2$ and assigns this state to the $\eta_b(2S)$, which corresponds to $\Delta M_{\text{HF}}(2S) = [48.6 \pm 3.1] \text{ MeV}/c^2$. This disagrees with most of the predictions for $\Delta M_{\text{HF}}(2S)$ from unquenched lattice calculations, potential models and a model-independent relation that are compiled in Ref. [5] and therefore suggests a flaw in the theoretical understanding of QCD hyperfine mass splittings. In contrast, the Belle result [3] is consistent with the theoretical expectations in Ref. [5].

In this Letter, we report a search for the states $X_{b\bar{b}}$ in $\Upsilon(2S) \rightarrow X_{b\bar{b}}\gamma$ decays and $\eta_b(1S)$ in $\Upsilon(2S) \rightarrow \eta_b(1S)\gamma$ decays using a data sample with an integrated luminosity of 24.7 fb^{-1} collected at the $\Upsilon(2S)$ peak with the Belle detector [6] at the KEKB asymmetric-energy e^+e^- collider [7]. The sample contains $(157.8 \pm 3.6) \times 10^6$ $\Upsilon(2S)$ decays [8], which is about 17 times larger than the one used in Ref. [4]. In addition, $1.7 [89.5] \text{ fb}^{-1}$ of data recorded 30 [60] MeV below the $\Upsilon(2S)$ [$\Upsilon(4S)$] resonance energy (“off-resonance”) are used to model the $e^+e^- \rightarrow q\bar{q}$ continuum background. It is not possible to reconstruct the $\eta_b(2S)$ state using exclusive reconstruction of the hadronic final state near the mass found in Ref. [3] because this region suffers from a low photon detection efficiency and high background.

We employ the EVTGEN [9] package to generate signal Monte Carlo (MC) events. The radiative decays of the $\Upsilon(2S)$ are generated using the helicity amplitude formalism [10]. Hadronic decays of the $(b\bar{b})$ system are modeled assuming a phase space distribution; to incorporate final state radiation effects, an interface to PHOTOS [11] is added. Inclusive $\Upsilon(2S)$ MC events, produced using PYTHIA [12] with the same luminosity as the data, are investigated for potential peaking backgrounds.

The Belle detector [6] is a large-solid-angle spectrometer that includes a silicon vertex detector, a 50-layer central drift chamber (CDC), an array of aerogel threshold Cherenkov counters (ACC), time-of-flight scintillation counters (TOF), and an electromagnetic calorimeter (ECL) comprising CsI(Tl) crystals. All these components are located inside a superconducting solenoid coil that provides a 1.5 T magnetic field.

Our event reconstruction begins with the selection of an appropriate number and type of charged particles to reconstruct a subset of the many exclusive hadronic final states of the $(b\bar{b})$ system. We restrict ourselves to the 26 modes reported in Ref. [4]: $2(\pi^+\pi^-)$, $3(\pi^+\pi^-)$, $4(\pi^+\pi^-)$, $5(\pi^+\pi^-)$, $K^+K^-\pi^+\pi^-$, $K^+K^-2(\pi^+\pi^-)$, $K^+K^-3(\pi^+\pi^-)$, $K^+K^-4(\pi^+\pi^-)$,

$2(K^+K^-)$, $2(K^+K^-)\pi^+\pi^-$, $2(K^+K^-\pi^+\pi^-)$, $2(K^+K^-)3(\pi^+\pi^-)$, $\pi^+\pi^-p\bar{p}$, $2(\pi^+\pi^-)p\bar{p}$, $3(\pi^+\pi^-)p\bar{p}$, $4(\pi^+\pi^-)p\bar{p}$, $\pi^+\pi^-K^+K^-p\bar{p}$, $2(\pi^+\pi^-)K^+K^-p\bar{p}$, $3(\pi^+\pi^-)K^+K^-p\bar{p}$, $K_s^0K^\pm\pi^\mp$, $K_s^0K^\pm\pi^\mp\pi^+\pi^-$, $K_s^0K^\pm\pi^\mp 2(\pi^+\pi^-)$, $K_s^0K^\pm\pi^\mp 3(\pi^+\pi^-)$, $2K_s^0(\pi^+\pi^-)$, $2K_s^0 2(\pi^+\pi^-)$, and $2K_s^0 3(\pi^+\pi^-)$.

We require all charged tracks, except for those from K_s^0 decays, to originate from the vicinity of the interaction point (IP) by requiring their impact parameters along and perpendicular to the z axis to be less than 4 and 1 cm, respectively. Here, the z axis is defined by the direction opposite the e^+ beam. Track candidates are identified as pions, kaons, or protons (“hadrons”) based on information from the CDC, the TOF and the ACC. The kaon identification efficiency is 83% – 91% with a pion misidentification probability of 8% – 10%. Pions are detected with an efficiency of 87% – 89% with a kaon-to-pion misidentification rate of 7% – 13%. The proton identification efficiency is 95%, while the probability of a kaon being misidentified as a proton is below 3%. Candidate K_s^0 mesons are reconstructed by combining two oppositely charged tracks (with a pion mass assumed for both) with an invariant mass between 486 and 509 $\text{ MeV}/c^2$; the selected candidates are also required to satisfy the criteria described in Ref. [13] to ensure that their decay vertices are displaced from the IP.

We then combine a photon candidate with the $(b\bar{b})$ system to form an $\Upsilon(2S)$ candidate. The photon is reconstructed from an isolated (not matched to any charged track) cluster in the ECL that has an energy greater than 22 MeV and a cluster shape consistent with an electromagnetic shower: the energy sum of the 3×3 array of crystals centered around the most energetic one exceeding 85% of that of the 5×5 array of crystals. The energy of the signal photon is 30 – 70 MeV and 400 – 900 MeV for the $X_{b\bar{b}}$ and $\eta_b(1S)$, respectively. We exclude photons from the backward endcap in the $\eta_b(1S)$ selection to suppress low-energy photons arising from beam-related background. For the $X_{b\bar{b}}$ selection, both the backward and forward endcap regions are excluded as the energy of the photon from the $\Upsilon(2S) \rightarrow X_{b\bar{b}}\gamma$ decay is too low, and lies in a range contaminated with large beam backgrounds. The photon energy resolution in the barrel ECL ranges between 2% at $E_\gamma = 1 \text{ GeV}$ and 3% at $E_\gamma = 100 \text{ MeV}$.

There is a weak correlation between the signal photon momentum and the thrust axis of the hadrons of the $(b\bar{b})$ system if the latter has spin zero. The same correlation is stronger for continuum events [2], so the cosine of the angle θ_T between the candidate photon and the thrust axis, calculated in the e^+e^- center-of-mass (CM) frame, is useful in suppressing the continuum background. Since the distribution of this variable is independent of the $(b\bar{b})$ -mass region considered, we require $|\cos\theta_T| < 0.8$ for a substantial reduction (60%) of continuum events and a modest loss (20%) of signal.

The signal windows for the difference between the en-

ergy of the $\Upsilon(2S)$ candidate and the CM energy (ΔE) and the $\Upsilon(2S)$ momentum measured in the CM frame ($P_{\Upsilon(2S)}^*$) are optimized separately for the $X_{b\bar{b}}$ and $\eta_b(1S)$ mass regions. We perform this optimization using a figure-of-merit $S/\sqrt{S+B}$, where S is the expected signal based on MC simulations, and B is the background estimated from a sum of the $\Upsilon(4S)$ off-resonance data, scaled to the available $\Upsilon(2S)$ integrated luminosity, and the inclusive $\Upsilon(2S)$ MC sample described earlier. The value of S is calculated by assuming the branching fraction to be 46.2×10^{-6} for the $X_{b\bar{b}}$ [4] and 3.9×10^{-6} for the $\eta_b(1S)$ [14]. The $\Upsilon(2S)$ candidates with $-40 \text{ MeV} < \Delta E < 50 \text{ MeV}$ and $P_{\Upsilon(2S)}^* < 30 \text{ MeV}/c$ [$-30 \text{ MeV} < \Delta E < 80 \text{ MeV}$ and $P_{\Upsilon(2S)}^* < 50 \text{ MeV}/c$] are retained for a further study of the $X_{b\bar{b}}$ [$\eta_b(1S)$] state. For the two-body decay hypothesis, the angle $\theta_{(b\bar{b})\gamma}$ between the reconstructed $(b\bar{b})$ system and the photon candidate in the CM frame should be close to 180° . We apply an optimized requirement on $\theta_{(b\bar{b})\gamma}$ to be greater than 150° [177°] to select the $\Upsilon(2S) \rightarrow X_{b\bar{b}}\gamma$ [$\Upsilon(2S) \rightarrow \eta_b(1S)\gamma$] decay candidates. The difference between the invariant mass formed by combining the signal photon with another photon candidate in the event and the nominal π^0 mass [15] is computed for each photon pair; the smallest of the magnitudes of these differences is denoted by $\Delta M_{\gamma\gamma}$ and used for a π^0 veto. For the $\eta_b(1S)$ selection, where the background contribution is dominated by π^0 's coming from the $\Upsilon(2S)$ decays, we require $\Delta M_{\gamma\gamma} > 10 \text{ MeV}/c^2$. We do not apply the π^0 veto in the $X_{b\bar{b}}$ selection since there is negligible π^0 contamination; the background here is dominated by photons coming from beam background. The final selection efficiencies for the individual modes range from 6.1% [$X_{b\bar{b}} \rightarrow 3(\pi^+\pi^-)$] to 1.2% [$X_{b\bar{b}} \rightarrow 2K_s^0 3(\pi^+\pi^-)$].

We apply a kinematic fit to the $\Upsilon(2S)$ candidates constrained by energy-momentum conservation. The resolution of the reconstructed invariant mass of the $\eta_b(1S)$, presented in terms of $\Delta M \equiv M[(b\bar{b})\gamma] - M(b\bar{b})$, is significantly improved by this fit from approximately 14 to $8 \text{ MeV}/c^2$. The improvement in the mass resolution is minimal for the $X_{b\bar{b}}$ since the photon has so little energy. The fit χ^2 value is used to select the best $\Upsilon(2S)$ candidate in the case of multiple candidates that appear in about 10% of the events satisfying the $X_{b\bar{b}}$ selection.

We extract the signal yield by performing an unbinned extended maximum-likelihood fit to the ΔM distribution for all selected candidates. The probability density functions (PDFs) for $\chi_{bJ}(1P)$ and $X_{b\bar{b}}$ signals are parametrized by the sum of a Gaussian and an asymmetric Gaussian function to take into account low-energy tails. Their parameters (the common mean, three widths, and the relative fraction) are taken from MC simulations. To account for the modest difference in the detector resolution between data and simulations, we use a calibration factor common to the four signal components, *i.e.*,

$\chi_{bJ}(1P)$ with $J = 0, 1, 2$ and $X_{b\bar{b}}$, to smear their core Gaussian components. The choice of the background

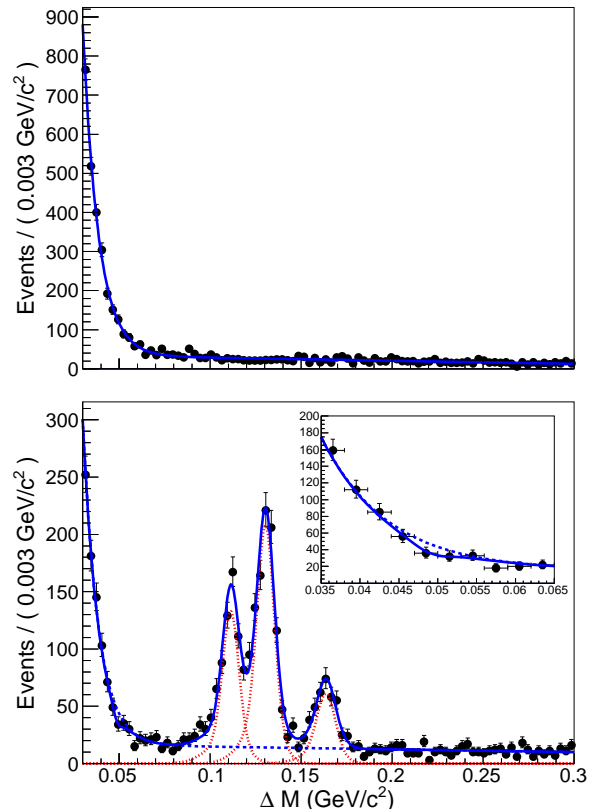


FIG. 1: (color online). The ΔM distributions for (top) $\Upsilon(4S)$ off-resonance data and (bottom) $\Upsilon(2S)$ data events that pass the selection criteria applied for the $[0.03, 0.30] \text{ GeV}/c^2$ region. Points with error bars are the data, (top) the blue solid curve is the result of the fit for the background-only hypothesis, and (bottom) the result of the fit for the signal-plus-background hypothesis, where blue solid and blue dashed curves are total fit and background components, respectively. The three $\chi_{bJ}(1P)$ components indicated by the red dotted curves are here considered as part of the signal. The bottom inset shows an expanded view of the ΔM distribution in the $[0.035, 0.065] \text{ GeV}/c^2$ region.

PDF is particularly important and is determined from the large sample of $\Upsilon(4S)$ off-resonance data. As shown in the top plot of Fig. 1, the best fit to these data is obtained by using a sum of an exponential function and a first-order Chebyshev polynomial for the $X_{b\bar{b}}$ region, whose parameters are allowed to vary in the fit. This is in contrast to Ref. [4], where a single exponential function was used to describe the background PDF. The polynomial component is needed to model the background due to final-state radiation for $\Delta M < 0.15 \text{ GeV}/c^2$ and from π^0 for $\Delta M \geq 0.15 \text{ GeV}/c^2$. We have verified using a large number of pseudoexperiments that if the $X_{b\bar{b}}$ signal is present in our data sample we would observe it with a significance above 10 standard deviations.

In the bottom plot of Fig. 1, we present fits to the ΔM distributions for the sum of the 26 modes in the $X_{b\bar{b}}$ region. The results of the fit show no evidence of an $X_{b\bar{b}}$ signal, with a yield of -30 ± 19 events. In the fits to the $\chi_{bJ}(1P)$ ($J = 0, 1, 2$) states we observe large signal yields and determine invariant masses of 9859.6 ± 0.5 , 9892.8 ± 0.2 and 9912.0 ± 0.3 MeV/c^2 , respectively, which are in excellent agreement with the corresponding world-average values [15]. The strong $\chi_{bJ}(1P)$ signals determine the aforementioned data-MC width-calibration factor to be 1.23 ± 0.05 . The parameters obtained for the background PDF in the $\Upsilon(2S)$ sample are consistent with those found in the fit to the $\Upsilon(4S)$ off-resonance data, giving us confidence in our background modeling.

The signal PDF for the $\eta_b(1S)$ is a Breit-Wigner function, whose width is fixed to the value obtained in Ref. [3], convolved with a Gaussian function with a width of $8 \text{ MeV}/c^2$ describing the detector resolution. A first-order Chebyshev polynomial is used for the background in the $\eta_b(1S)$ region, validated with the large sample of $\Upsilon(4S)$ off-resonance data. The result of the fit to off-resonance data is presented in the top plot of Fig. 2. No signal (-6 ± 10 events) is found for the $\eta_b(1S)$, as shown in the bottom plot of Fig. 2.

For a particle of mass near $10 \text{ GeV}/c^2$, exclusive decays are distributed across many final states, and thus we use the $\chi_{b0}(1P)$ [spin-zero, as for the $\eta_b(nS)$] decay modes for guidance. The average efficiency for each $(b\bar{b})$ state is calculated with the individual efficiencies $[\varepsilon_{(b\bar{b})}^i]$ obtained with MC samples weighted according to the yields $[N_{\chi_{b0}(1P)}^i]$ for each mode in the $\chi_{b0}(1P)$ case, as

$$\varepsilon[(b\bar{b})] = \sum_{i=1}^{26} \frac{\varepsilon_{(b\bar{b})}^i \times N_{\chi_{b0}(1P)}^i}{N_{\chi_{b0}(1P)}^{\text{tot}}}, \quad (1)$$

where $N_{\chi_{b0}(1P)}^{\text{tot}}$ denotes the total sum of the signal yields obtained for the 26 hadronic decays of the $\chi_{b0}(1P)$. Those efficiencies are corrected to take into account the data-MC difference in the hadron identification efficiency. The corrected efficiencies are 2.9% and 3.5% for the $X_{b\bar{b}}$ and $\eta_b(1S)$, respectively. Very similar results are obtained when using the $\chi_{b1}(1P)$ or $\chi_{b2}(1P)$ state as the proxy instead of the $\chi_{b0}(1P)$.

We estimate the uncertainties on the signal yields due to the signal PDF shapes using $\pm 1\sigma$ variations of the shape parameters that are fixed in the fit. The dominant sources of such additive systematic errors are the $X_{b\bar{b}}$ [4] and $\eta_b(1S)$ [3] masses. For the upper limit estimates (described below), we conservatively use the fit likelihood, which gives the largest upward variation of the signal yield: 18 and 4 events for the $X_{b\bar{b}}$ and $\eta_b(1S)$, respectively. The multiplicative systematic uncertainties that do not affect the signal yields are summarized in Table I. The largest contribution arises from the uncertainty in the efficiency estimate. Two sources dominate here: (a) the statistical error in the yield of the

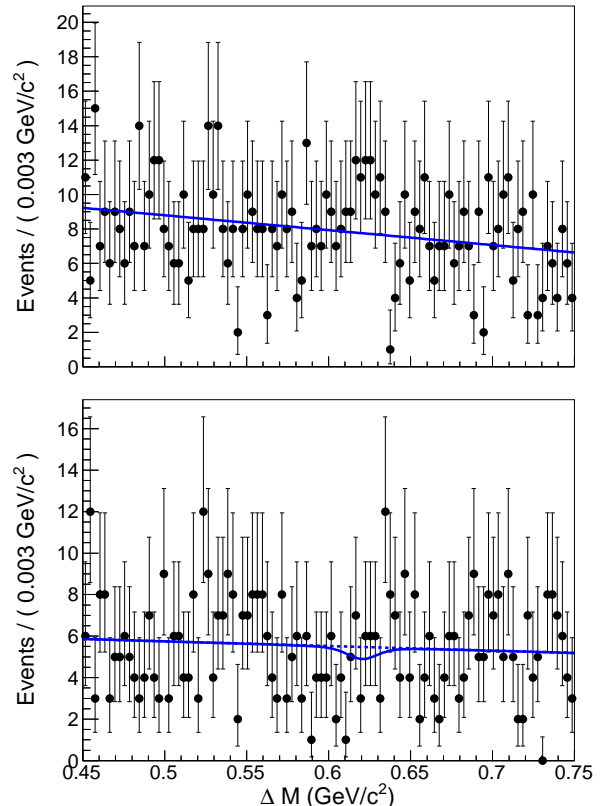


FIG. 2: (color online). The ΔM distributions for (top) $\Upsilon(4S)$ off-resonance data and (bottom) $\Upsilon(2S)$ data events that pass the selection criteria applied for the $[0.45, 0.75] \text{ GeV}/c^2$ region. Points with error bars are the data, (top) the blue solid curve is the result of the fit for the background-only hypothesis, and (bottom) the result of the fit for the signal-plus-background hypothesis, where blue solid and blue dashed curves are total fit and background components, respectively.

different decay modes of the $\chi_{b0}(1P)$ and (b) the effects of possible intermediate states on the signal efficiency (referred to as “decay modeling”). As described earlier, all our signal MC samples are generated with a phase space distribution. Therefore, in order to estimate the contribution from source (b), possible intermediate states such as $\rho^0 \rightarrow \pi^+\pi^-$, $K^*(892)^0 \rightarrow K^+\pi^-$ and $K^*(892)^\pm \rightarrow K_s^0\pi^\pm$ are considered. Differences in the efficiencies based on the same final-state modes generated with these intermediate resonances can be as large as 9.2%. The other minor sources arise from hadron identification, charged track reconstruction, K_s^0 and photon detection, and the number of $\Upsilon(2S)$.

The branching fraction is determined from the number of observed signal events (n_{sig}) as $\mathcal{B} = n_{\text{sig}} / \{\varepsilon[(b\bar{b})] \times N_{\Upsilon(2S)}\}$, where $\varepsilon[(b\bar{b})]$ is evaluated according to Eq. (1) and $N_{\Upsilon(2S)}$ is the total number of $\Upsilon(2S)$ decays. In the absence of the signal, we obtain an upper limit at 90% confidence level (C.L.) on the branching fraction

TABLE I: Multiplicative systematic uncertainties (in %) considered in the estimation of the $X_{b\bar{b}}$ and $\eta_b(1S)$ upper limits.

Source	$X_{b\bar{b}}$	$\eta_b(1S)$
Efficiency calculation	± 2.5	± 2.9
Decay modeling	± 9.2	± 6.9
Hadron identification	± 3.7	± 3.7
Track reconstruction	± 2.6	± 2.6
K_S^0 detection	± 0.2	± 0.2
Photon detection	± 3.0	± 3.0
Number of $\Upsilon(2S)$	± 2.3	± 2.3
Total	± 11.2	± 9.5

(\mathcal{B}_{UL}) by integrating the likelihood (\mathcal{L}) of the fit with fixed values of the branching fraction: $\int_0^{\mathcal{B}_{\text{UL}}} \mathcal{L}(\mathcal{B}) d\mathcal{B} = 0.9 \times \int_0^1 \mathcal{L}(\mathcal{B}) d\mathcal{B}$. Multiplicative systematic uncertainties are included by convolving the likelihood function with a Gaussian function with a width equal to the total uncertainty. We estimate $\mathcal{B}[\Upsilon(2S) \rightarrow \eta_b(1S)\gamma] \times \sum_i \mathcal{B}[\eta_b(1S) \rightarrow h_i] < 3.7 \times 10^{-6}$ and $\mathcal{B}[\Upsilon(2S) \rightarrow X_{b\bar{b}}\gamma] \times \sum_i \mathcal{B}[X_{b\bar{b}} \rightarrow h_i] < 4.9 \times 10^{-6}$.

In summary, we have searched for the $X_{b\bar{b}}$ state reported in Ref. [4], that is reconstructed in 26 exclusive hadronic final states using a sample of $(157.8 \pm 3.6) \times 10^6$ $\Upsilon(2S)$ decays. We find no evidence for a signal and thus determine a 90% C.L. upper limit on the product branching fraction $\mathcal{B}[\Upsilon(2S) \rightarrow X_{b\bar{b}}\gamma] \times \sum_i \mathcal{B}[X_{b\bar{b}} \rightarrow h_i] < 4.9 \times 10^{-6}$, which is an order of magnitude smaller than the branching fraction reported in Ref. [4]. We have also searched for the $\eta_b(1S)$ state and set an upper limit $\mathcal{B}[\Upsilon(2S) \rightarrow \eta_b(1S)\gamma] \times \sum_i \mathcal{B}[\eta_b(1S) \rightarrow h_i] < 3.7 \times 10^{-6}$ at 90% C.L.

We thank the KEKB group for excellent operation of the accelerator; the KEK cryogenics group for efficient solenoid operations; and the KEK computer group, the NII, and PNNL/EMSL for valuable computing and SINET4 network support. We acknowledge support from MEXT, JSPS and Nagoya's TLPRC (Japan); ARC and DIISR (Australia); FWF (Austria); NSFC (China);

MSMT (Czechia); CZF, DFG, and VS (Germany); DST (India); INFN (Italy); MEST, NRF, GSDC of KISTI, and WCU (Korea); MNiSW and NCN (Poland); MES and RFAAE (Russia); ARRS (Slovenia); IKERBASQUE and UPV/EHU (Spain); SNSF (Switzerland); NSC and MOE (Taiwan); and DOE and NSF (U.S.).

-
- [1] N. Brambilla *et al.*, Eur. Phys. J. C **71**, 1534 (2011).
 - [2] B. Aubert *et al.* (BABAR Collaboration), Phys. Rev. Lett. **101**, 071801 (2008); **102**, 029901(E) (2009).
 - [3] R. Mizuk *et al.* (Belle Collaboration), Phys. Rev. Lett. **109**, 232002 (2012).
 - [4] S. Dobbs, Z. Metreveli, A. Tomaradze, T. Xiao and K.K. Seth, Phys. Rev. Lett. **109**, 082001 (2012).
 - [5] T. J. Burns, Phys. Rev. D **87**, 034022 (2013).
 - [6] A. Abashian *et al.* (Belle Collaboration), Nucl. Instrum. Methods Phys. Res., Sect. A **479**, 117 (2002); also, see the detector section in J. Brodzicka *et al.*, Prog. Theor. Exp. Phys.04D001 (2012).
 - [7] S. Kurokawa and E. Kikutani, Nucl. Instrum. Methods Phys. Res., Sect. A **499**, 1 (2003), and other papers included in this volume; T. Abe *et al.*, Prog. Theor. Exp. Phys., 03A001 (2013) and following articles up to 03A011.
 - [8] X. L. Wang *et al.* (Belle Collaboration), Phys. Rev. D **84**, 071107(R) (2011).
 - [9] D. J. Lange, Nucl. Instrum. Methods Phys. Res., Sect. A **462**, 152 (2001).
 - [10] M. Jacob and G. C. Wick, Ann. Phys. (N.Y.) **7**, 404 (1959); Ann. Phys. (N.Y.) **281**, 774 (2000).
 - [11] E. Barberio and Z. W̧as, Comput. Phys. Commun. **79**, 291 (1994); P. Golonka and Z. W̧as, Eur. Phys. J. C **45**, 97 (2006); **50**, 53 (2007).
 - [12] T. Sjöstrand, S. Mrenna, and P. Skands, Comput. Phys. Commun. **178**, 852 (2008).
 - [13] K.-F. Chen *et al.* (Belle Collaboration), Phys. Rev. D **72**, 012004 (2005).
 - [14] B. Aubert *et al.* (BABAR Collaboration), Phys. Rev. Lett. **103**, 161801 (2009).
 - [15] J. Beringer *et al.* (Particle Data Group), Phys. Rev. D **86**, 010001 (2012).